

Rational Design of Femtomolar Inhibitors of Isoleucyl tRNA Synthetase from a Binding Model for Pseudomonic Acid-A

Murray J. B. Brown,[‡] Lucy M. Mensah,[‡] Michael L. Doyle,[§] Nigel J. P. Broom,^{||} Neal Osbourne,^{||} Andrew K. Forrest,^{||} Christine M. Richardson,^{||} Peter J. O'Hanlon,^{||} and Andrew J. Pope^{*,‡}

Departments of Molecular Recognition, Medicinal Chemistry, and Structural Biology, SmithKline Beecham, New Frontiers Science Park, Harlow, Essex, U.K., and King of Prussia, Pennsylvania

Received January 24, 2000; Revised Manuscript Received March 24, 2000

ABSTRACT: This paper describes the design and characterization of novel inhibitors of IleRS, whose binding affinity approaches the tightest reported for noncovalent inhibition. Compounds were designed from a binding model for the natural product pseudomonic acid-A (PS-A) together with a detailed understanding of the reaction cycle of IleRS and characterization of the mode of binding of the reaction intermediate IleAMP. The interactions of the compounds with IleRS were characterized by inhibition of aminoacylation of tRNA or PP_i/ATP exchange at supersaturating substrate concentration and by transient kinetics and calorimetry methods. A detailed understanding of the interaction of a comprehensive series of compounds with IleRS allowed the identification of key features and hence the design of exquisitely potent inhibitors. Predictions based on these results have been recently supported by a docking model based on the crystal structure of IleRS with PS-A [Silvian, L. F., Wang J. M., and Steitz T. A. (1999) *Science* 285 1074–1077].

The aminoacyl tRNA synthetases catalyze the esterification of amino acids to cognate tRNA molecules (2). Despite common features in terms of the catalytic chemistry required, these enzymes display a wide range of molecular structures, and moreover, considerable divergence has occurred over time such that the prokaryotic enzymes exhibit low sequence homology with respect to their eukaryotic counterparts (3). Given the lack of sequence similarity and also that the aminoacylation process is essential in all living organisms, these enzymes make attractive antibacterial targets against which to develop compounds that selectively inhibit the prokaryotic synthetase and the design of such inhibitors has attracted much theoretical and practical interest (4, 5). A number of tRNA synthetase inhibitors are known, including substrate analogues (6, 7) and natural products (8–14). An important demonstration of the potential of this approach is shown by mupirocin (pseudomonic acid-A, PS-A),¹ which specifically inhibits bacterial isoleucyl tRNA synthetases while being ca. 10000-fold less potent against the corresponding mammalian enzyme (15, 16). This drug is currently the world's most widely used topical antibiotic and has been studied extensively in this laboratory as reported previously (17–19) together with reaction intermediate mimetics (Ile-ol-AMP and Ile-NHSO₂-AMP) and other pseudomonic acid analogues. Arising from these findings and in the context of

data describing the complete reaction cycle for IleRS (18), we developed a binding model for PS-A inhibition of IleRS and, from this model, designed IleRS inhibitors that have potency comparable to the tightest noncovalent enzyme inhibitors previously reported. The rational design of enzyme inhibitors is usually fuelled by the availability of structural data, but a detailed knowledge of reaction kinetics and inhibitor binding kinetics and thermodynamics is of great value. In this case structural data was obtained after the event and has been used to corroborate the experimental findings.

PS-A structurally resembles the reaction intermediate IleAMP in several respects and it was initially proposed that the dihydroxytetrahydropyran ring of the monate is analogous to the ribose moiety of the adenylate, with the α,β -unsaturated ester mimicking adenine. This model would therefore place the epoxide-containing side chain in the same site as the amino acid. However, the side chain does not represent a particularly good mimic of isoleucine in either a steric or electronic sense, lacking the zwitterion of the aminoacyl phosphate and having apparently incorrect separation between the ring and amino acid side-chain moieties. Since the binding model proposes that PS-A resembles the catalytic intermediate IleAMP, it predicts that PS-A should bind to the same enzyme form as the adenylate. Indeed, steady-state kinetic experiments showed that PS-A was competitive with both Ile and ATP. Additionally, binding of PS-A and stable adenylate analogues (Ile-ol-AMP, Ile-NHSO₂-AMP) was shown to be mutually exclusive (17). However, consideration of the conformations adopted by the inhibitor–protein complex as reported by analysis of changes in intrinsic tryptophan fluorescence indicated that the modes of binding of the two classes must be different (17). Steady-state IleRS Trp fluorescence measurements in the presence of excess inhibi-

* To whom correspondence should be addressed. Phone: 0 12 79 62 75 83. Fax: 0 12 79 62 75 99. E-mail: Andrew_J_Pope@SBPHRD.COM.

[‡] Department of Molecular Recognition.

[§] Department of Structural Biology, King of Prussia.

^{||} Department of Medicinal Chemistry.

¹ Abbreviations: IleRS, isoleucyl tRNA synthetase; PS-A, pseudomonic acid-A; Et-A, ethyl monate; PP_i, inorganic pyrophosphate; IleAMP, isoleucyl adenylate; Ile-ol-AMP, isoleucyl adenylate; Ile-NHSO₂-AMP, isoleucyl sulfamoyladenylate; SAR, structure activity relationship.

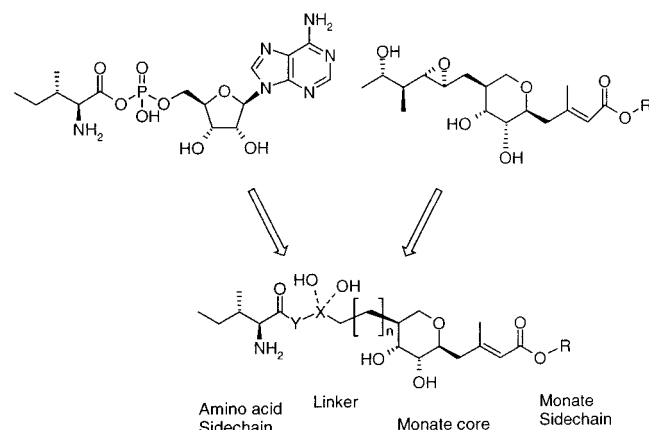


FIGURE 1: Design for combination of features of reaction intermediate and monate inhibitors to produce more potent hybrid inhibitor.

tor showed that while the adenylate analogues produce a 15–17% enhancement of fluorescence (identical to that seen with catalytically produced IleAMP), binding of monates to IleRS produces a much smaller, but consistent, 1–2% change. Further evidence that the mode of binding of the two classes differs was provided by the fact that the monates show time-dependent inhibition with a slow tightening step after initial binding whereas the adenylates show classical rapid equilibrium inhibition (17). This indicates that although the binding site of the monates overlaps with that of the adenylate intermediate, there are considerable differences in enzyme:inhibitor conformation. These differences were presumed to be due to the amino acid binding site being unoccupied by the monate inhibitors. It was, therefore, hypothesized that the binding energy used to stabilize the reaction intermediate, as evidenced by the change in tryptophan environment, could be expropriated to provide for greater potency in the monate-based inhibitors by appropriate modification. The key question was to identify optimal moieties to combine to produce a high-affinity chimera.

Four pharmacophores were identified within the chimeric aminoacyl monate structure (Figure 1). In this paper, we describe the systematic optimization of these pharmacophores resulting in exquisitely potent compounds approaching the tightest noncovalent inhibitors reported. The monate core, comprising the dihydroxytetrahydropyran and 3-methylacrylate moieties, was regarded as essential to provide selectivity for bacterial over mammalian IleRSs and was consequently retained. Variation of the amino acid side chain and linker allowed exploration of molecular interactions within the IleRS active site. Variation of the monate side chain will be discussed elsewhere.

MATERIALS AND METHODS

IleRS and Other Reagents. IleRS from *S. aureus* was purified (to >98% as judged by SDS–PAGE or reversed-phase HPLC) from *Escherichia coli* DH1 cells carrying the pDB575 plasmid (20) and shown to be fully active by active-site titration performed either through the measurement of a burst of Mg.ATP utilization (21) or the measurement of the stoichiometric IleRS:[¹⁴C]IleAMP complex by gel filtration. Except where otherwise stated, reagents were of the highest grade available and purchased mainly from Sigma (Poole, Dorset, U.K.).

Inhibitors. Pseudomonic acid-A (PS-A) and ethyl monate-A (Et-A) were isolated from producing *Pseudomonas fluorescens* strains as described (22). All other compounds (with SB numbers) were prepared by SmithKline Beecham and fully characterized by at least ¹H NMR and HR-MS. Synthetic details will be published elsewhere.

IleRS and Steady-State Enzyme Kinetics. tRNA aminoacylation and PP_i/ATP exchange assays were performed by the methods previously reported (17). Using the microscopic rate constants derived for the complete reaction cycle, we had previously shown that IC₅₀ values were linearly related to the dissociation constant (*K_i*). Under the conditions used, the derived factors are *K_i* = IC₅₀(PP_i/ATP exchange)/2300 = IC₅₀(aminoacylation)/3.2.

Stopped-Flow/Steady-State Fluorescence Measurements. These were performed as previously reported (17). Second-order association rate constants were calculated by linear regression of *k_{obs}* vs [inhibitor] plots.

Kinetic Data Analysis. Stopped-flow kinetic time courses were analyzed using the nonlinear least-squares fitting routines supplied by Applied Photophysics. All other least-squares fitting was performed using GRAFIT (23). Kinetic simulation was performed using the MS-DOS version of KINSIM (24) or the Windows NT version of GESPAISI (25, 26).

Calorimetry and Thermal Stability. Inhibitor-binding affinities were determined by a two-part thermodynamic approach (27, 28). (1) The IleRS stabilization energy due to inhibitor binding was measured from differences in IleRS unfolding energies. Differential scanning calorimetry (DSC) was used to measure the required (eq 1) unfolding thermodynamics [enthalpy and heat capacity changes, and half-unfolded (*T_m*) temperatures] of IleRS in the absence of inhibitors. In the presence of inhibitors, only the *T_m* values were needed to determine the stabilization energies. Thus, circular dichroism (CD) melting measurements were used because the method uses less material than DSC. (2) The stabilization energies, which yield the *K_d* values at elevated temperatures, were then corrected to 25 °C from isothermal titration calorimetry (ITC) measurements of inhibitor binding enthalpy and heat capacity changes using the integrated Van't Hoff equation as described elsewhere (29).

Thermodynamic measurements were made in 5 mM Hepes, pH 7.4, 150 mM NaCl, and 1 mM MgCl₂. DSC measurements were made with a Calorimetry Sciences Corporation (Provo, Utah) NanoDSC calorimeter at a scan rate of 1 °C/min. CD thermal stability measurements were made with a JASCO J-710 spectropolarimeter at a scan rate of 1 °C/min. ITC measurements were made with a Microcal MCS microcalorimeter.

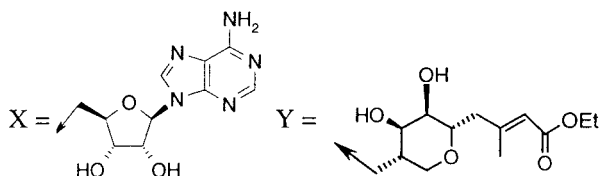
Inhibitor dissociation constants at the melting temperatures were calculated using eq 1 (27).

$$K_d^{T_{ml}} = \frac{[I_{tot}] - \frac{[IleRS]}{2}}{\left[\frac{\Delta H_U}{R} \left(\frac{1}{T_{ml}} - \frac{1}{T_{mO}} \right) + \frac{\Delta C_{p,U}}{R} \left(\ln \frac{T_{ml}}{T_{mO}} + \frac{T_{mO}}{T_{ml}} - 1 \right) \right] - 1} \quad (1)$$

Here, *T_{ml}* is the unfolding *T_m* of IleRS in the presence of the

Table 1: Dependence of K_i on Variations in Linker Region

Compound	Structure	K_i (nM) ^a	Compound	Structure	K_i (nM)
Ile-ol-AMP		50	SB-239945		2.0
Ile-NHSO ₂ -AMP		0.01	SB-252180		0.4
Et-A		0.19	SB-251109		900
SB-224736		0.02	SB-246096		0.04
SB-234764		<0.001	SB-254412		0.6
SB-226371		1.4	SB-239171		420



^a K_i calculated from inhibition of either aminoacylation of tRNA or PP_i/ATP exchange (see Materials and Methods)

inhibitor, and $K_d^{T_{ml}}$ is the inhibitor equilibrium dissociation constant at the T_{ml} . T_{m0} is the T_m of IleRS in the absence of inhibitor, ΔH_U is the unfolding enthalpy of IleRS at T_0 , and $\Delta C_{p,U}$ is the unfolding heat capacity change. ΔH_U was measured by DSC, whereas $\Delta C_{p,U}$, which is a second-order temperature correction to ΔH_U , was approximated as -3 kcal/mol/°C from protein unfolding studies (30) due to low signal-to-noise in the present DSC data. $[I_{Tot}]$ and $[IleRS]$ are the total concentrations of inhibitor and IleRS, respectively, and R is the universal gas constant. The dissociation constants were then calculated as a function of temperature with the integrated van't Hoff equation to determine values at 25 °C (29).

Modeling Studies. All modeling work was carried out using the CHARMM 97 force field with visualization of the structures using Quanta (31). The structure of the *Staphylococcus aureus* isoleucyl tRNA synthetase enzyme, in complex with pseudomonic acid-A and tRNA, was received from Steitz and co-workers (1) in advance of its publication. This was used as a basis for the modeling work. The tRNA was removed, and hydrogens were added to the protein and the ligand using CHARMM. The PS-A was removed and then a minimization routine, based on a combination of the steepest descents and adopted-basis Newton Raphson algorithms, was used, in conjunction with explicit solvation and flexibility of both the active site and the ligand, to prepare a docking model. The model was tested by returning the

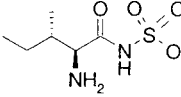
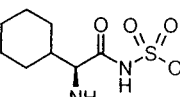
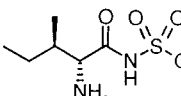
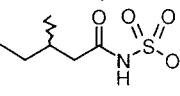
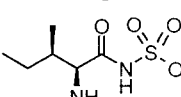
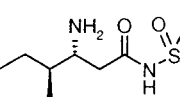
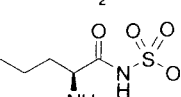
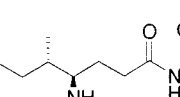
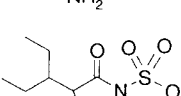
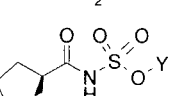
PS-A to the active site and minimizing. This verified that the docking routine produced sensible results. This process was repeated using a model of the isoleucyl adenylate as the ligand and this produced a modeled complex which was in good agreement with the starting enzyme conformation and with the conformation of the aminoacyl adenylate consistent with that recognized by other class I aminoacyl tRNA synthetase enzymes.

The structure of SB-234764 was built and initially aligned within the constraints of the active site in a conformation broadly consistent with the bound conformations of isoleucyl adenylate and pseudomonic acid-A. It was then subjected to the same docking routine and the minimized complexes of the pseudomonic acid-A, the isoleucyl adenylate and the SB-234764 ligands, were compared.

RESULTS

Optimization of the Linker. By analogy with the adenylate analogues studied previously (17) both phosphate and sulfamate-based linkers were used. Ethyl monophosphate (Et-A) was used as the template for these designed inhibitors due to synthetic accessibility. The length and polarity of the linker was varied both to probe direct interactions with the active site and in order to allow the Ile side chain to occupy its binding pocket. A number of analogues were made (32), and the key compounds are shown in Table 1 together with K_i parameters derived from either inhibition of aminoacylation

Table 2: Dependence of K_i on the Amino Acid Side Chain Composition

Compound	Structure	K_i (nM)	Compound	Structure	K_i (nM)
SB-234764		<0.001	SB-247186		0.55
SB-239820		0.7	SB-236838		6900
SB-241083		4.8	SB-244519		0.31
SB-251803		0.007	SB-248453		55
SB-255183		0.56	SB-244151		230

Y = see Table 1

of tRNA or, for more potent compounds, inhibition of the PP_i/ATP exchange reaction in the presence of supersaturating substrates (see Materials and Methods). All the compounds with the monate core were found to show time-dependent inhibition, indicating that it is not the epoxide containing side chain that is responsible for further tightening after initial binding.

The first point to note is that the best chimeric inhibitor SB-234764 exceeds the tight-binding limit even in the presence of supersaturating substrate concentrations and that this represents more than 2 orders of magnitude greater affinity than the parent compounds. This construct has about the same distance between the Ile side chain and the dihydroxytetrahydropyran ring as between the Ile and ribose in the adenylates, indicating that the two rings probably do indeed occupy the same site on IleRS. Modeling studies are in good agreement with this, showing that the isoleucyl adenylate and SB-234764 can adopt similar binding modes within the active site cleft, although the orientations of the sugar rings do differ.

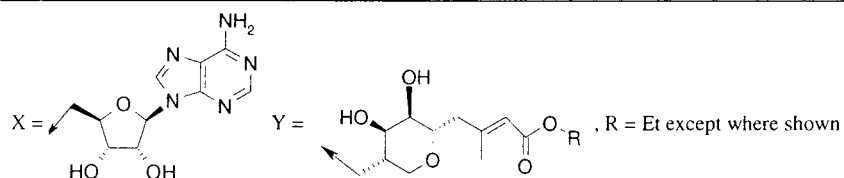
Increasing the distance between the isoleucine and the sugar moiety (as in SB-226371) reduces potency dramatically. It is also apparent that sulfamate is a better linking moiety than phosphate. This mirrors the finding in the adenylate analogues where the sulfamate, Ile-NHSO₂-AMP, is approximately 4 orders of magnitude more potent than the phosphate, Ile-ol-AMP. Replacement of the sulfamate by phosphate (SB-224736) resulted in a loss of potency of more than an order of magnitude. It is notable that the phosphate linker lacks the aminoacyl carbonyl group and, interestingly, deletion of the carbonyl function in the sulfamate (SB-239945) results in even greater loss of affinity, indicating that this group provides a major contribution to the affinity. Confirmation of the importance of the isoleucyl carbonyl group is found in the comparison of the two sulfamides (SB-252180 and SB-251109) where deletion causes a loss of affinity greater than 3 orders of magnitude.

A high degree of sensitivity was also shown to the polarity of the linking moiety. The series SB-234764, SB-252180, SB-246096, and SB-254412 maintain the spatial distance between the monate core and isoleucyl group but alter the polarity of the linker (it must be noted that changes to the ground-state conformation cannot be excluded). Replacement of the linking oxygen by a methylene to give the sulfonamide (SB-246096) causes a substantial loss of affinity. Substitution by nitrogen to give sulfamide (SB-252180) brings about a further order of magnitude decrease in potency and replacement of both linking heteroatoms by methylenes yielding the sulfone (SB-254412) produces a similar loss of affinity. This indicates that the stereoelectronic properties of the sulfamate are optimal and this may represent a transition-state analogue for the phosphoanhydride during adenylation. A further observation is that the active site will not accommodate the isoleucyl-monate with N-methylation at the linker (SB-239171), though whether this is due to steric or electronic factors is unclear. Modeling studies do suggest that the NH packs well against the active-site surface and that a hydrogen-bonding interaction is possible with the backbone of Pro 56. However, it should be remembered that the NH proton is likely to be acidic and may not be present at physiological pH.

Exploration of Amino Acid Binding Pocket. The aminoacyl moiety was also varied, in part to explore the IleRS active site and incidentally to determine if the strategy would allow inhibition of other tRNA synthetases. The foregoing data established the optimal linking group as the sulfamate, and this structure was generally kept constant. Table 2 summarizes a selection of the relevant data. Encouragingly, the natural amino acid (L-Ile) substitution was found to be the optimal moiety, consistent with our hypothesis that the aminoacyl monate inhibitors exploit the amino acid binding pocket. As might be expected, there was strong selectivity for the correct stereochemistry for the amino acid, with Ile isomers (e.g., SB-239820 and SB-241083) showing a marked

Table 3: Equilibrium Trp Fluorescence Enhancement of IleRS Complexes with Inhibitors and Microscopic Rate Constants Derived from Stopped Flow Mixing Experiments

Compound	Structure	ΔF (%)	k_{on} ($\mu M^{-1}s^{-1}$)	Compound	Structure	ΔF (%)	k_{on} ($\mu M^{-1}s^{-1}$)
PS-A		1.7	10.2	SB-226371		2	1
Et-A		2	1.3	SB-244519		6.7	2.9
Ile-ol-AMP		16.1	2.4	SB-223142		16	0.9
Ile-NHSO ₂ ⁻ AMP		16.0	9.0	SB-227425		11	0.84
SB-234764		14.9	1.4	SB-225339		4.9	1.96
SB-224736		16	1.5	SB-223923		1.8	1.5
				SB-236996		16	12



decrease in affinity. Deletion of the branched Me (SB-251803) was reasonably well tolerated, but addition of steric bulk, e.g., the β -ethyl (SB-255183) or the constrained cyclohexyl (SB-247186) analogues, was detrimental to affinity. Deletion of the α -amino group (SB-236838) was found to be very detrimental to activity.

The strict requirement for appropriate spacing found in the linker region was found to apply equally in the aminoacyl portion. Introduction of methylenes (SB-244519 and SB-248453) between the amino group and the carbonyl caused a rapid and significant loss of affinity.

The tight constraints on both the amino acid and the linker, favoring the natural L-Ile structure and the sulfamate predicted to be most like that in the intermediate adenylate, add weight to our hypothesis as to the binding model for pseudomonic acid-A and for the aminoacyl monates described here.

Alternative natural amino acid side chains were also examined (e.g., Pro, SB-244151). Interestingly, although activity vs IleRS was much reduced relative to SB-234764, the level of activity vs the cognate tRNA synthetase was much poorer still, indicating the specificity of the monate structure for IleRS.

Binding Mode of Aminoacyl Monates. Although the increase in potency shown by SB-234764 over the parent compounds, and the SAR seen, is a necessary consequence of our binding hypothesis, it does not prove that the Ile-binding pocket is occupied and that the extra binding energy obtained comes from arrogation of the energy associated with the conformational change induced during catalysis. Evidence that this was the case was obtained from observation of the change in steady-state IleRS fluorescence on binding (Table 3). Monate compounds with the epoxide containing side chain (e.g., PS-A and Et-A) show a very small fluorescence

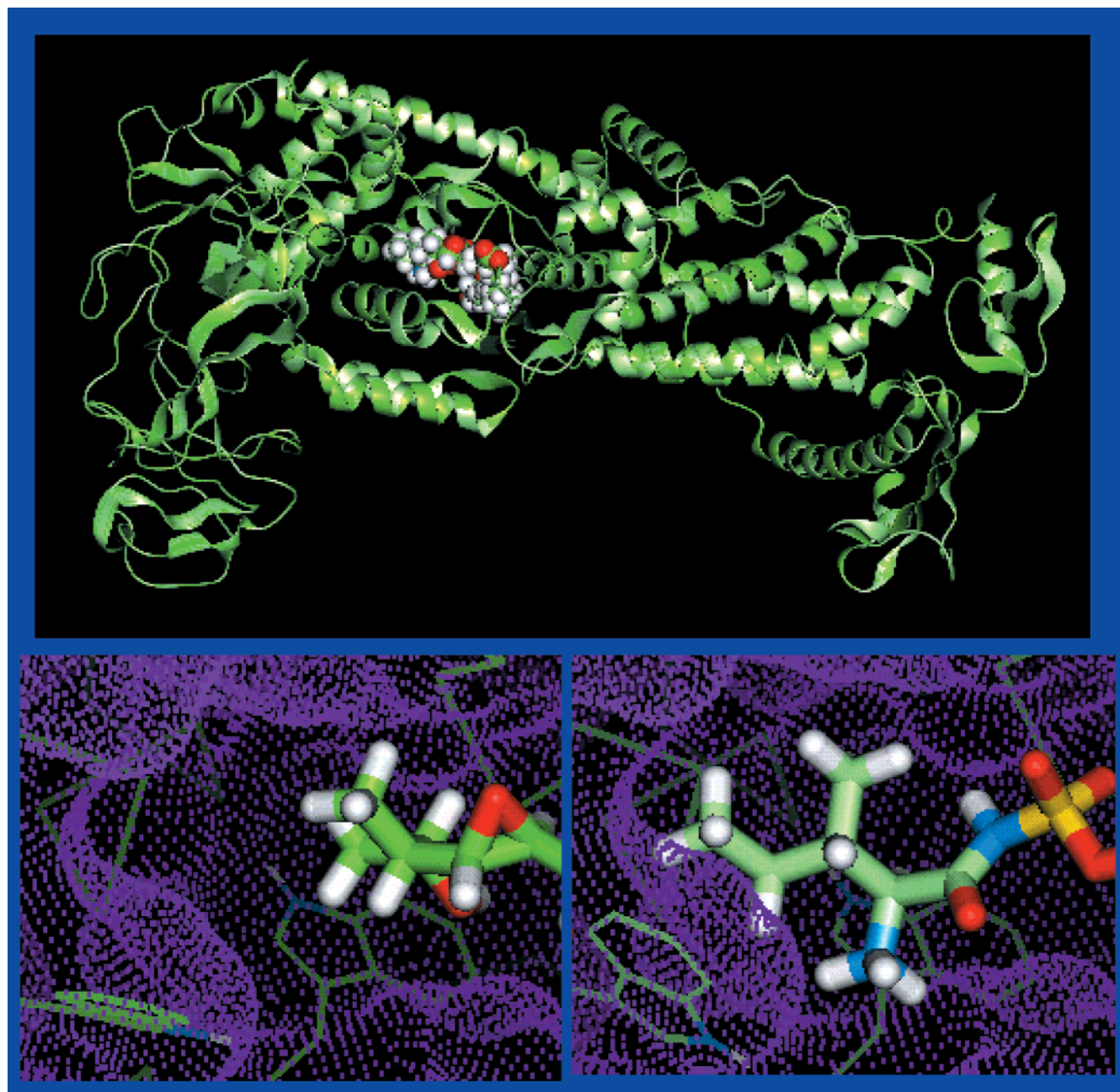


FIGURE 2: Upper panel shows the secondary structure of the isoleucyl tRNA synthetase enzyme and the overlapping binding sites for the minimized PS-A and the modeled SB-234764. The ligands are shown in space fill representation, with the carbon atoms of the PS-A being shown in dark green while those of SB-234764 are shown in light green. The lower panels show detailed views of the isoleucine binding pocket, where the purple dots represent the solvent accessible surface and the protein is shown in wireframe, as an α -carbon representation plus tryptophan side chains. Fragments of each of the respective ligands are shown in liquorice representation. The isoleucine binding pocket is bordered by two tryptophan residues which are solvent exposed in the PS-A complex (left-hand panel) but which pack against the side chain in the SB-234764 complex (right-hand panel).

enhancement ($\sim 2\%$) whereas the intermediate analogues Ile-ol-AMP and Ile-NHSO₂-AMP show a much larger (16%) change. The aminoacyl monate chimeric compounds with the correct amino acid side chain (SB-234764 and SB-224736) showed a 15–16% enhancement of IleRS fluorescence upon binding, almost identical to that seen during catalytic turnover (18) and with the adenylate analogues (Ile-ol-AMP and Ile-NHSO₂-AMP) (e.g., Figure 3). This is strong evidence that the chimeric inhibitor induces the same enzyme conformation as seen during turnover. Further evidence that this is dependent upon the appropriate amino acid side chain is shown by the fact that structures predicted to be less

suitable generate a smaller increase in enzyme fluorescence and that the increase is qualitatively related to the similarity to L-Ile. Introduction of an extra methylene between the sulfamate and the ring (SB-226371) eliminates the additional fluorescence enhancement, whereas extension of the amino acid side chain by a single methylene series (SB-244519) only reduces the fluorescence enhancement to $\sim 7\%$, indicating a limited degree of flexibility in the amino acid binding site beyond the linker binding site. Interestingly, in analogous compounds with a phosphate linker, an extra methylene inserted between the phosphate and the ring *and* the opposite stereochemistry at the β -methyl (SB-223142) still gives the

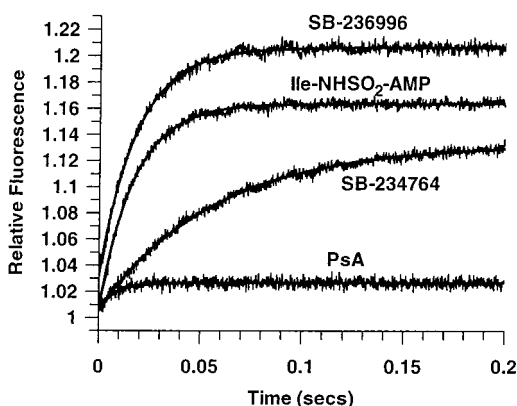


FIGURE 3: Trp fluorescence transients for inhibitor binding to IleRS. Stopped flow traces for rapid mixing of IleRS (100 nM) with 10 μ M inhibitor as shown. Data for SB-236996 is offset by 0.04 RFU for clarity.

maximum fluorescence enhancement. As noted previously, compounds with a phosphate linker are significantly less potent than those with a sulfamate linker, it may be that the lack of the Ile carbonyl removes a conformational restriction on the compound allowing occupation the Ile-binding pocket. In the series with phosphate linkers, the fluorescence enhancement was found to decrease in the series Ile > Val (SB-227425) > Met (SB-225339) > Tyr (SB-223923), the last showing no difference from the parent Et-A. This series of compounds again illustrates that it is occupation of the Ile-binding pocket that causes the conformational change reported by the fluorescence enhancement. Again it was found that addition of a different amino acid side chain (other than Ile) did not produce an inhibitor of the cognate tRNA synthetase, demonstrating the specificity of the monate structure for IleRS.

The differences in tryptophan fluorescence observed between the PS-A complex and the SB-234764 complex are consistent with modeling results. The crystal structure of the isoleucyl tRNA synthetase:PS-A complex shows that the proposed isoleucine-binding site is bordered by two tryptophan residues, Trp 528 and Trp 562. These residues can be seen in Figure 2 and are largely solvent exposed when PS-A is bound, as can be observed in the lower left panel.

A corresponding view of the modeled SB-234764 complex is shown in the lower right panel of Figure 2. The amino acid binding pocket has been filled with the isoleucine side chain, which makes good hydrophobic interactions with both of the tryptophan aromatic rings. This modification of the local environment of the tryptophan residues would be expected to enhance their fluorescence yield, as observed on binding of the Ile-containing compounds. In addition, a favorable hydrogen-bonding arrangement can be seen between the SB-234764 amino group and the side chain of Gln 558. This Gln side chain is also involved in a hydrogen bond through to the carbonyl group, in good agreement with the SAR data. This is also in agreement with the data on the crystallographically observed *Thermus thermophilus* isoleucine complex, as published by Nureki et al. (33). However, these workers also observe a salt bridge between Asp 85 of the *T. thermophilus* enzyme and the isoleucine amino group. This interaction does not appear to be made in the modeled complex of SB-234764 in the *S. aureus* homologue.

Transient Binding Kinetics of Optimum Inhibitors. It was noted above that SB-234764 gave tight binding in the PP_i exchange assay so the K_i reported in Table 1 can only provide an upper estimate. However, the chimeric compounds produced a significant enhancement of Trp fluorescence on binding to IleRS, so it was possible to characterize them by measurement of the microscopic rate constants for binding using transient kinetics. It can be seen that the on-rate for the compounds (Table 3) is constant for the aminoacyl ethylmonates at about $1\text{--}3 \times 10^6 \text{ M}^{-1} \text{ s}^{-1}$ independent of potency, and that increased potency is largely as a result of a slower off-rate and an increase in the forward equilibrium for the subsequent tightening step. For these very potent compounds, the overall off-rates were found to be too slow to be measurable by the techniques previously developed to study the parent monates and the adenylate analogues (17).

It had previously been shown that PS-A was approximately 10-fold more potent than Et-A ($K_i = 0.017$ vs 0.19 nM), so it was surmised that addition of the full nonanoic acid pseudomonate side chain to SB-234764, to give SB-236996, might increase the potency of the chimera still further. SB-236996 was again observed to be tight binding in the PP_i exchange assay, so although no loss of potency was seen, it was impossible to tell if potency had increased. However, transient kinetics had shown that the association rate constant for PS-A ($10.2 \times 10^6 \text{ M}^{-1} \text{ s}^{-1}$) was about 7 times faster than for Et-A ($1.3 \times 10^6 \text{ M}^{-1} \text{ s}^{-1}$). Gratifyingly a similar effect was seen in the chimeric compounds (Figure 3) with the Et-A analogue, SB-234764 ($1.4 \times 10^6 \text{ M}^{-1} \text{ s}^{-1}$), slower than the PS-A analogue, SB-236996 ($1.2 \times 10^7 \text{ M}^{-1} \text{ s}^{-1}$), indicating that an increase in potency had probably been achieved. To quantify the binding affinity to IleRS, the complexes were investigated by isothermal calorimetry and enhanced stability analysis.

Measurement of K_d by Thermal Stability. To quantify the potency of the chimeric compounds that were tight binding under the lowest enzyme concentration and highest substrate concentration usable for activity measurements, we turned to thermodynamic methods. This involved measuring each inhibitor's stabilization energy of IleRS by DSC and CD melting. The melting temperature (T_m) for IleRS in the absence of inhibitor was determined by DSC as 52°C , and the unfolding enthalpy change was measured as 75 kcal/mol at 52°C . The unfolding heat capacity change was approximated from previous protein folding studies as $3 \text{ kcal/mol}^\circ\text{C}$ (30) due to the low signal-to-noise of the present data set. The magnitude of the ΔH_U is smaller than expected for a 106 kDa protein and suggests that we are measuring inhibitor stabilization energies of a subdomain portion of IleRS. In fact, both DSC and CD melting in the absence of inhibitor indicated two unfolding transitions for IleRS (T_m values of 52 and 70°C). The present analysis determines inhibitor binding affinities with a single-domain binding and folding model and uses the 52°C transition as the relevant unfolding domain since this is the one that is predominantly stabilized. However, for the extremely tight inhibitors, stabilization of both unfolding domains is observed, suggesting an inhibitor-induced interdomain stabilization mechanism. In these cases, the estimated affinities may be weaker than the true affinities by amounts related to the increased stability of the 70°C unfolding domain.

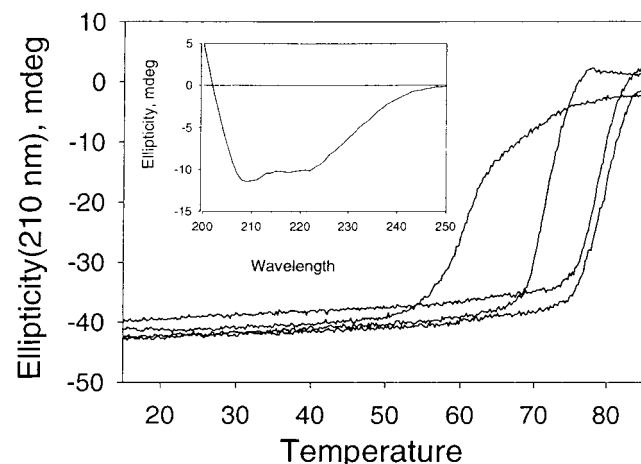


FIGURE 4: Stabilization of IleRS by binding of various inhibitors. Raw data ellipticity at 210 nm is shown versus temperature ($^{\circ}\text{C}$). Unfolding of IleRS is accompanied by an increase in ellipticity at 210 nm as expected for a loss in secondary structure. A representative set of unfolding curves for several inhibitors are shown (from left to right: Ile-ol-AMP, Ile-NHSO₂-AMP, SB-234764, and SB-236996). Inset: CD spectrum of IleRS in the absence of inhibitors at 15 $^{\circ}\text{C}$, 5 mM Hepes, pH 7.4, 150 mM NaCl, 1 mM MgCl₂ and 0.25 mg/mL IleRS. Optical path was 0.1 cm.

Table 4: Calorimetry Parameters for Binding and Stabilization of IleRS by Inhibitors

compd	K_d at 25 $^{\circ}\text{C}$ (pM)	IleRS T_m ($^{\circ}\text{C}$)	ΔH at 25 $^{\circ}\text{C}$ (kcal/mol)	ΔC (kcal/ mol deg)
control	NA	52	NA	NA
Ile-ol-AMP	40 000	60.2	-7	ND
Et-A	250	66.8	-17	-0.37
PS-A	140	69.5	-15	ND
Ile-NHSO ₂ -AMP	15	71.9	-12	-0.31
SB-234764	0.012	78.8	-17	-0.53
SB-236996	0.010	80.0	-18	-0.37

Melting temperatures in the presence of inhibitors were measured by CD spectroscopy (Figure 4) and the T_m s were used to calculate the K_d values for each inhibitor at their respective melting temperatures (eq 1). The K_d values at 25 $^{\circ}\text{C}$ were then calculated from the inhibitor binding thermodynamics as measured by ITC using the integrated Van't Hoff equation (29).

The results in Table 4 show that IleRS is stabilized to different extents in the presence of various inhibitors. The extent of stabilization is in turn related to the affinity of each inhibitor by the thermodynamic relationships described above. Table 4 also lists the affinities for each inhibitor as determined from the thermal stability analysis. The results correlate well for those compounds for which the PP_i exchange assay did not show tight binding (Figure 5). However, the tight binding limit in the PP_i/ATP exchange reaction is approximately ~ 1 pM, so for the two tightest inhibitors, the K_d values could only be determined by calorimetry. For these inhibitors, SB-234764 and SB-236996, the K_d values near 10 fM are exceptionally tight. The addition of the full PS-A side chain to the aminoacyl monate in SB-236996 increases the T_m slightly to 80 $^{\circ}\text{C}$; however, the relative affinities of SB-234764 and SB-236996 are experimentally indistinguishable at this level. Clearly, the potency of these compounds is approaching the limits of resolvability of the CD method, and it is thus possible that, based on the

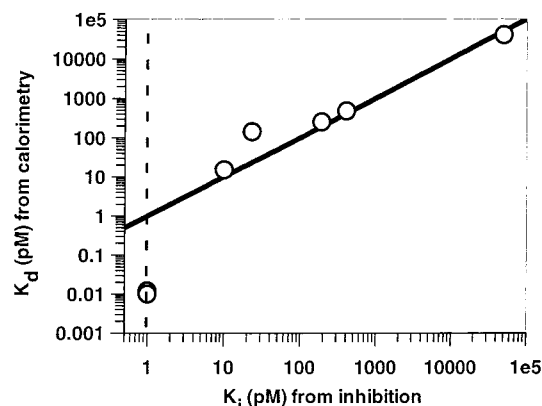


FIGURE 5: Correlation between K_i calculated from ATP/PP_i exchange IC₅₀ value (x -axis) and K_d calculated by calorimetry (y -axis). Solid line represents expected correlation ($K_d = K_i$) between values for compounds not showing tight binding in ATP/PP_i exchange assay. Dotted line shows the tight binding limit in ATP/PP_i exchange assay.

enhanced on-rate, the 10 fM figure for SB-236996 may be an underestimate.

DISCUSSION

Inhibition of tRNA synthetase activity is a clinically validated mechanism for antibiotic action, and development of novel inhibitors is a potential route to circumventing the growing problem of antibiotic resistance. The design and synthesis of potent and selective inhibitors is an essential prerequisite for the development of antimicrobial chemotherapy. To optimize the potency, a detailed understanding of inhibitor binding and enzyme action is required for the rational improvement of existing inhibitors. The inhibitors described in this paper were designed from our initial hypothesis for a binding model for PS-A based on a detailed understanding of the reaction cycle of IleRS and its interactions with intermediate analogues and monate inhibitors. The binding model can be summarized as follows: (a) the binding site of PS-A overlaps with that of IleAMP, such that the dihydroxytetrahydropyran and ribose rings overlap but the epoxide containing side chain does not occupy the Ile-binding pocket; (b) occupation of the Ile-binding pocket induces an inhibitor:IleRS complex in which Trp fluorescence is enhanced; (c) extra binding energy can be achieved by appropriate introduction of an Ile moiety to improve the potency of monate-based inhibitors.

This binding model allowed the design of inhibitors that are among the most potent noncovalent enzyme inhibitors reported to date. It has been shown that introduction of an Ile side chain with appropriate spacing to the monate dihydroxytetrahydropyran ring gives precisely the predicted Trp fluorescence enhancement. This additional enhancement correlates with a marked increase in potency. The recent publication of a crystal structure of IleRS with PS-A cocrystallized at the active site has allowed the examination of these results at the atomic level (1).

The X-ray structure shows that the epoxide side chain of PS-A falls short of the proposed Ile-binding pocket which is lined with two tryptophans. Modeling work suggests that when the Ile side chain is present (in either IleAMP or the aminoacyl monates) the Ile group lies against the face of one of the tryptophans (Trp 528) with an excellent hydro-

phobic contact and makes a greatly improved contact with the other (Trp 562). There does not appear to be a major conformational change required to allow IleAMP or aminoacyl monates to bind, so the tryptophan hydrophobic contact and exclusion of water from the solvent exposed face appears sufficient to give the fluorescence enhancement seen. The increase in potency appears to be due to a combination of good hydrophobic interactions with the isoleucyl side chain of the inhibitor, displacing ordered water molecules, and also due to improved hydrogen bonding between the ligand and the enzyme. It is likely that these interactions are also important in the selective binding of the cognate amino acid.

In addition, examination of a range of inhibitors demonstrates that a major binding interaction is apparent with the aminoacyl carbonyl of IleAMP and analogues. The crystal structure shows that there is a perfectly aligned Gln(Gln 558), 1.8 Å from the Ile carbonyl which provides a rationale for the importance of the aminoacyl carbonyl for optimal potency.

This paper demonstrates that detailed understanding of the kinetics and thermodynamics of substrate and inhibitor interactions to the level of determination of microscopic rate constants, combined with an interrogation of protein:ligand conformations by intrinsic Trp fluorescence yields can allow the rational design of inhibitor molecules several orders of magnitude more potent than the starting compounds. The potency of the inhibitors described here are at the limits of quantification even using sophisticated calorimetry techniques. The preparation of a comprehensive range of closely related inhibitors provides a wealth of information on substrate- and inhibitor-binding determinants in an approach that complements more conventional site directed mutagenesis of active site residues to identify key interactions between the protein and ligand.

ACKNOWLEDGMENT

We would like to thank Pamela Brown, John Elder, Peter Milner, Donna Pengelly and Graham Walker (SmithKline Beecham) for their contributions to the synthesis of the compounds reported in this paper. We are also very grateful to Tom Steitz and co-workers for early access to the structural data for the PS-A:IleRS complex.

REFERENCES

- Silvian, L. F., Wang, J. M., and Steitz, T. A. (1999) *Science* 285, 1074–1077.
- Meinzel, T., Mechulam, Y., and Blanquet, S. (1995) in *tRNA, structure, biosynthesis and function* (Soll, D., and RajBhandary, U. L., Eds.) pp 251–292, ASM Press, Washington DC.
- Carter, C. W., Jr. (1993) *Annu. Rev. Biochem.* 62, 715–748.
- von der Haar, F., Gabius, H.-J., and Cramer, F. (1981) *Angew. Chem., Int. Ed. Engl.* 20, 217–223.
- Schimmel, P., Tao, J., and Hill, J. (1998) *FASEB J.* 12, 1599–1609.
- Biryukov, A. I., Zhukov, Yu.-N., Lavrik, O. I., and Khomutov, R. M. (1990) *FEBS Lett.* 273, 208–210.
- Laske, R., Schonenberger, H., Holler, E. (1989) *Arch. Pharm.* 322, 847–852.
- Nass, G., Poralla, K., and Zahner, H. (1969) *Biochim. Biophys. Acta* 34, 84–91.
- Paetz, W., and Nass, G. (1973) *Eur. J. Biochem.* 35, 331–333.
- Tanaka, K., Tamoki, M., and Watanabe, S. (1969) *Biochim. Biophys. Acta* 195, 244–245.
- Ogilvie, A., Wiebauer, K., and Kersten, W. (1975) *Biochem. J.* 152, 511–515.
- Werner, R. G., Thorpe, L. F., Reuter, W., and Nierhaus, K. H. (1976) *Eur. J. Biochem.* 68, 1–3.
- Konrad, I., and Roschenthaler, R. (1977) *FEBS Lett.* 83, 341–347.
- Konishi, M., Nishio, M., Saitoh, K., Miyaki, T., Oki, T., and Kawaguchi, H. (1989) I. Production, isolation, physicochemical properties and structure. *J. Antibiot. (Tokyo)* 42, 1749–1755.
- Hughes, J., and Mellows, G. (1978) *J. Antibiot.* 31, 330–335.
- Hughes, J., and Mellows, G. (1980) *Biochem. J.* 191, 209–219.
- Pope, A. J., Moore, K. J., McVey, M., Mensah, L., Benson, N., Osbourne, N., Broom, N., Brown, M. J. B., and O'Hanlon, P. (1998) *J. Biol. Chem.* 273, 31691–31701.
- Pope, A. J., Lapointe, J., Mensah, L., Brown, M. J. B., Benson, N., and Moore, K. J. (1998) *J. Biol. Chem.* 273, 31680–31690.
- Pope, A. J., McVey, M., Fantom, K., and Moore, K. J. (1998) *J. Biol. Chem.* 273, 31702–31706.
- Chalker, A. F., Ward, J. M., Fosberry, A. P., and Hodgson, J. E. (1994) *Gene* 141, 103–108.
- Fersht, A. R. (1984) *Enzyme Structure and Mechanism*, ISBN 7167-1614, Freeman & Company, New York.
- Fuller, A. T., Mellows, G., Woodford, M., Banks, G. T., Barrow, K. D., and Chain, E. B. (1971) *Nature* 234, 416–417.
- Leatherbarrow, R. (1992) Erithacus Software Ltd., London.
- Barshop, B. A., Wrenn, R. F., and Freiden, C. (1983) *Anal. Biochem.* 130, 134–145.
- Mendes, P. (1993) *Comput. Appl. Biosci.* 9, 563–571.
- Mendes, P. (1997) *Trends Biochem. Sci.* 22, 361–363.
- Brandts, J. F., and Lin, L.-N. (1990) *Biochemistry* 29, 6927–6940.
- Weber, P. C., Pantoliano, M. W., Simons, D. M., Salemme, F. R. (1994) *J. Am. Chem. Soc.* 116, 2717–2724.
- Doyle, M. L., and Hensley, P. (1998) *Method Enzymol.* 295, 88–99.
- Privalov, P. L., and Khechinashvili, N. N. (1974) *J. Mol. Biol.* 86, 665–684.
- Quanta available from Molecular Simulations Inc, 9685, Scranton Road, San Diego, CA, 92121-3752, <http://www.msi.com>.
- Forrest, A. K., Pengelly, D., and O'Hanlon, P. J. WO 97/05126.
- Nureki, O., Vassilyev, D. G., Tateno, M., Shimada, A., Nakama, T., Fukai, S., Konno, M., Hendrickson, T., Schimmel, P., Yokoyama, S. (1998) *Science* 280, 578–582.

BI000148V